Draft version November 4, 2016
Preprint typeset using LaTeX style AASTeX6 v. 1.0

arXiv:1606.08855v3 [astro-ph.EP] 3 Nov 2016

HIDING PLANETS BEHIND A BIG FRIEND: MUTUAL INCLINATIONS OF MULTI-PLANET SYSTEMS WITH EXTERNAL COMPANIONS

Dong Lai and Bonan Pu
Cornell Center for Astrophysics and Planetary Science, Department of Astronomy, Cornell University, Ithaca, NY 14853, USA

ABSTRACT

The *Kepler* mission has detected thousands of planetary systems with 1-7 transiting planets packed within 0.7 au from their host stars. There is an apparent excess of single-transit planet systems that cannot be explained by transit geometries alone, when a single planetary mutual inclination dispersion is assumed. This suggests that the observed compact planetary systems have at least two different architectures. We present a scenario where the "Kepler dichotomy" may be explained by the action of an external giant planet or stellar companion misaligned with the inner multi-planet system. The external companion excites mutual inclinations of the inner planets, causing such systems to appear as "Kepler singles" in transit surveys. We derive approximate analytic expressions (in various limiting regimes), calibrated with numerical calculations, for the mutual inclination excitations for various planetary systems and perturber properties (mass m_p, semi-major axis a_p and inclination θ_p). In general, the excited mutual inclination increases with m_p/a_p^3 and θ_p, although secular resonances may lead to large mutual inclinations even for small θ_p. We discuss the implications of our results for understanding the dynamical history of transiting planet systems with known external perturbers.

Keywords: planetary systems — planets and satellites: dynamical evolution and stability — planets and satellites: formation — stars: individual (Kepler-48, Kepler-56, Kepler-68, Kepler-444, Kepler-454, WASP-47, GJ 832, 55 Cancri)

1. INTRODUCTION

NASA's *Kepler* mission has discovered ~ 4700 planet candidates (as of May 2016), about half of which are confirmed planets (e.g. Mullally et al. 2015; Coughlin et al. 2016; Morton et al. 2016). Most of these planets are super-Earths or sub-Neptunes (with radii 1.2-3$R_\oplus$), and have orbital periods less than 200 days. Among the $n_{\rm tran} = 3606$ Kepler planetary systems, 80% have one transiting planet, and 20% have 2-7 transiting planets [The number of systems with $N_{\rm tran}$ planets is $n(N_{\rm tran}) = 2871, 492, 158, 61, 20, 3, 1$ for $N_{\rm tran} = 1, 2, \cdots, 7$].[1] The observed transit multiplicity distribution, $f(N_{\rm tran}) = n(N_{\rm tran})/n_{\rm tran}$, and its dependence on the sizes and periods of planets, contain useful information on the architecture of compact planetary systems, such as the true planet multiplicity, the mutual inclinations, and orbital spacings between adjacent planets. In general, there exists a degeneracy between these (underlying) quantities in producing the same $f(N_{\rm tran})$. For example, larger planet spacings and mutual inclinations will raise the relative number of single-transit systems (Lissauer et al. 2011; Tremaine & Dong 2012). This degeneracy can be partially lifted by combining the statistics of $f(N_{\rm tran})$ with the result of RV surveys (Tremaine & Dong 2012; Figueira et al. 2012), or using the transit duration ratios of different planets orbiting the same star (Fabrycky et al. 2014). The general conclusion from a number of studies is that Kepler compact planetary systems are flat, with the inclination dispersion of order a few degrees (Lissauer et al. 2011; Tremaine & Dong 2012; Figueira et al. 2012; Johansen et al. 2012; Fang & Margot 2012; Fabrycky et al. 2014).

It has been noted that models with a single mutual inclination dispersion (e.g. in a Rayleigh distribution) fall short in explaining the large number of single-transit ($N_{\rm tran} = 1$) systems relative to multiple-transit (higher-$N_{\rm tran}$) systems by a factor of two or more (Lissauer et al. 2011; Johansen et al. 2012; Weissbein et al. 2012; Ballard & Johnson 2016). [2] This suggests that the Kepler planetary systems may consist of at least two underlying populations with different architectures: The first has many ($\gtrsim 6$) planets with small ($\lesssim 2^\circ$) mutual inclinations, and accounts for the majority of the $N_{\rm tran} \geq 2$ systems; the second has fewer planets or higher mutual inclinations, and accounts for a significant portion of the observed single-transit systems. This is the so-

[1] Data was retrieved form the NASA Exoplanet Archive on May 17, 2016; planets with a KOI deposition "False Positive" were removed from this sample.

[2] This result depends somewhat on the assumed forms of the underlying multiplicity function (Tremaine & Dong 2012), since there is a degeneracy between the mutual inclination distribution and the multiplicity function.

called "Kepler Dichotomy". Xie et al. (2014) found that the multi-transit systems are more likely to exhibit detectable transit timing variations than the single-transit systems, suggesting that the former are more closely packed than the latter. Morton & Winn (2014) found that the obliquities of stars with a single transiting planet are systematically larger than those with multiple transiting planets (see Albrecht et al. 2013), again suggesting that a substantial fraction of Kepler's single-transit systems are dynamically hotter than the flat multiple-transit systems.

The origin of the Kepler dichotomy is unknown. The observed Kepler multi-planet systems appear to be tightly packed and close to the edge of instability (Fang & Margot 2013; Pu & Wu 2015; Volk & Gladman 2015). Thus a dichotomy in planetary architectures may arise from the long-term evolution of dynamically full systems. In this picture, the more densely packed systems underwent dynamical instability, leading to planet collision/consolidation and the formation of Kepler "singles" (Pu & Wu 2015; Volk & Gladman 2015). It is unclear to what extent dynamical instability can account for the Kepler dichotomy quantitatively, as the observed Kepler multi's are sufficiently "cold" and not massive enough to experience appreciable inclination excitation or dynamical instability within the stellar lifetime (Johansen et al. 2012; Becker & Adams 2016). On the other hand, the Kepler dichotomy may have a primordial origin, and results from the in-situ assembly of planetesimal disks (Hansen & Murray 2013) with different masses and density profiles (Moriarty & Ballard 2015).

In this paper we study the excitation of mutual inclinations in a compact multi-planet system by an external giant planet or stellar companion (Sections 2 and 3). In general, the giant planet may be on a misaligned orbit relative to the inner planetary system, as a result of warp in protoplanetary disks (e.g., Foucart & Lai 2011,2014) or strong scatterings between multiple giants (Juric & Tremaine 2008; Chatterjee et al. 2008). A distant stellar companion may also be inclined because of its misaligned orbital angular momentum at birth (e.g. Hale 1994). By exciting mutual inclinations of the inner planets, the giant planet can "heat up" the inner multi-planet system, causing it to appear as a single-transit system.

Since $\sim 50\%$ of the solar-type stars are in binaries, it is not surprising that many exoplanetary systems (including Kepler planet candidates) have been found to have external binary companions with a range of separations (e.g., Baranec et al. 2016). There is observational evidence that relatively close-by stellar companions (with separation $\lesssim 20-50$ au) tend to reduce the planet formation efficiency (e.g., Wang et al. 2015a; Kraus et al. 2016; Ngo et al. 2016). Wang et al. (2015b) found that $5\pm5\%$ of Kepler multi's have stellar companions at separation 1-100 au, compared to 21% for field stars in the solar neighborhood, suggesting that such companions can misalign or disrupt multi-planet systems. On the other hand, RV surveys continue to reveal a population of giant planets at large distances ($\gtrsim$ a few au) from their host stars (e.g., Marmier et al. 2013; Feng et al. 2015; Moutou et al. 2015; Rowan et al. 2016; Wittenmyer et al. 2016; Bryan et al. 2016). The Keck survey suggests that about 20% of solar-type stars could host gas giants within 20 au (Cumming et al. 2008), while HARPS finds that 14% of such stars host giant planets with periods less than 10 years. Because of the limited time span and the faint magnitudes of Kepler stars, the current census of distant giant companions to Kepler compact systems is rather incomplete. Nevertheless, a number of such long-period companions or candidates have been found using the transit method (Schmitt et al. 2014; Uehara et al. 2016) and the RV method (e.g., Kepler-48, Kepler-56, Kepler-68, Kepler-90, Kepler-454); a number of non-*Kepler* "inner compact planets + giant companion" systems have also been found (e.g., GJ 832, WASP-47) – see Section 4 for applications of our theory to some of these systems. Bryan et al. (2016) reported that about 50% of one and two-planet systems discovered by RV have companions in the 1-20M_J and 5-20 au range. All these results indicate that external ($\gtrsim 1$ au) giant planet companions are common around hot/warm ($\lesssim 1$ au) planets, and may significantly shape the architecture of the inner planetary systems.

We note that the possible role of external companions on compact planetary systems has often been noted (e.g. Lissauer et al. 2011) and formal secular theories (with various approximations) suitable for such study have been presented before (e.g. Tremaine et al. 2009; Boue & Fabrycky 2014). Our paper makes progress on this problem by deriving simple approximate analytic expressions (in various limiting regimes), calibrated with numerical results (Sections 2 and 3), that allow us to answer the question: Given an inner planetary system, what are the mutual inclinations excited by an external perturber of mass m_p, semi-major axis a_p and inclination θ_p? In general, a "strong" perturber (with large m_p/a_p^3) with high θ_p leads to larger mutual inclinations in the inner planets. But our work also reveals that under some conditions, large mutual inclinations can be generated even for small θ_p ($\lesssim 1^\circ$) because of secular resonances.

2. TWO-PLANET SYSTEMS WITH EXTERNAL PERTURBER

Consider two planets (mass m_1 and m_1) in circular orbits (semi-major axes a_1 and a_2, with $a_2 > a_1$) around a central star (mass $M_\star$). The two planets are initially coplanar. An external perturber (mass m_p) moves in a circular inclined orbit [3], with semi-major axis a_p (>

[3] When the perturber has an finite eccentricity e_p, we can simply replace a_p by $a_p\sqrt{1-e_p^2}$ in all equations to capture the leading quadrupole-order effect of the perturber on the planets (e.g., Liu et al. 2015).

a_1, a_2) and inclination angle θ_p. How does the mutual inclination of the two inner planets evolve?

We denote the angular momentum vectors to the three planets by $\boldsymbol{L}_1 = L_1\hat{\boldsymbol{l}}_1$, $\boldsymbol{L}_2 = L_2\hat{\boldsymbol{l}}_2$ and $\boldsymbol{L}_p = L_p\hat{\boldsymbol{l}}_p$, where $\hat{\boldsymbol{l}}_1$, $\hat{\boldsymbol{l}}_2$ and $\hat{\boldsymbol{l}}_p$ are unit vectors. When $L_p \gg L_1,\ L_2$, the unit vector $\hat{\boldsymbol{l}}_p$ is fixed in time. The evolution of $\hat{\boldsymbol{l}}_1$, $\hat{\boldsymbol{l}}_2$ is governed by

$$\frac{\mathrm{d}\hat{\boldsymbol{l}}_1}{\mathrm{d}t} = \omega_{12}(\hat{\boldsymbol{l}}_1\cdot\hat{\boldsymbol{l}}_2)(\hat{\boldsymbol{l}}_1\times\hat{\boldsymbol{l}}_2) + \Omega_{1p}(\hat{\boldsymbol{l}}_1\cdot\hat{\boldsymbol{l}}_p)(\hat{\boldsymbol{l}}_1\times\hat{\boldsymbol{l}}_p), \quad (1)$$

$$\frac{\mathrm{d}\hat{\boldsymbol{l}}_2}{\mathrm{d}t} = \omega_{21}(\hat{\boldsymbol{l}}_1\cdot\hat{\boldsymbol{l}}_2)(\hat{\boldsymbol{l}}_2\times\hat{\boldsymbol{l}}_1) + \Omega_{2p}(\hat{\boldsymbol{l}}_2\cdot\hat{\boldsymbol{l}}_p)(\hat{\boldsymbol{l}}_2\times\hat{\boldsymbol{l}}_p). \quad (2)$$

Here ω_{12} measures the precession rate of $\hat{\boldsymbol{l}}_1$ around $\hat{\boldsymbol{l}}_2$ (driven by m_2), and Ω_{1p} the precession rate of $\hat{\boldsymbol{l}}_1$ around $\hat{\boldsymbol{l}}_p$ (driven by m_p):

$$\omega_{12} = \frac{Gm_1m_2a_1}{4a_2^2L_1}b_{3/2}^{(1)}\left(\frac{a_1}{a_2}\right), \quad (3)$$

$$\Omega_{1p} = \frac{Gm_1m_pa_1}{4a_p^2L_1}b_{3/2}^{(1)}\left(\frac{a_1}{a_p}\right), \quad (4)$$

where $b_{3/2}^{(1)}(\chi)$ is the Laplace coefficient:

$$b_{3/2}^{(1)}(\chi) = \frac{2}{\pi}\int_0^\pi \frac{\cos\phi\,\mathrm{d}\phi}{(1-2\chi\cos\phi+\chi^2)^{3/2}}. \quad (5)$$

Similar expressions apply to ω_{21} and Ω_{2p}. Clearly

$$\frac{\omega_{21}}{\omega_{12}} = \frac{L_1}{L_2} = \frac{m_1}{m_2}\left(\frac{a_1}{a_2}\right)^{1/2}, \quad (6)$$

$$\frac{\Omega_{2p}}{\Omega_{1p}} = \left(\frac{a_2}{a_1}\right)^{1/2}\frac{b_{3/2}^{(1)}(a_2/a_p)}{b_{3/2}^{(1)}(a_1/a_p)}. \quad (7)$$

Note that Eqs. (1)-(4) are approximate but become exact in two limiting cases: (i) $\hat{\boldsymbol{l}}_1$, $\hat{\boldsymbol{l}}_2$ and $\hat{\boldsymbol{l}}_p$ are nearly aligned (e.g., Tremaine 1991); (ii) $\chi \ll 1$, in which case the quadrupole approximation is accurate and $b_{3/2}^{(1)}(\chi) = 3\chi[1 + (15/8)\chi^2 + (175/64)\chi^4 + \cdots] \simeq 3\chi$ (Murray & Dermott 1999).

2.1. *Numerical Result*

We integrate Eqs. (1)-(2) with an initially aligned pair of inner planets, and an inclined external perturber at $\theta_p = 10^\circ$. Figure 1 shows a few examples of the time evolution of the mutual inclination angle (θ_{12}) between the two inner planets, for $a_1 = 0.3$ au, $a_2 = 0.5$ au, $m_2/m_1 = 10$, and several values of ϵ_{12}, as defined by

$$\epsilon_{12} \equiv \frac{\Omega_{2p}-\Omega_{1p}}{\omega_{12}+\omega_{21}}. \quad (8)$$

Figure 2 depicts the maximum mutual inclination, $(\theta_{12})_{\rm max}$, as a function of ϵ_{12} for several different values of mass ratio m_2/m_1. The dimensionless parameter ϵ_{12} measures whether the inner planets are strongly coupled ($\epsilon_{12} \ll 1$) or weakly coupled ($\epsilon_{12} \gg 1$); see below. Note that ϵ_{12} can be written as

$$\epsilon_{12} = \hat{\Omega}_{1p}\,\frac{(\Omega_{2p}/\Omega_{1p})-1}{1+(L_1/L_2)}. \quad (9)$$

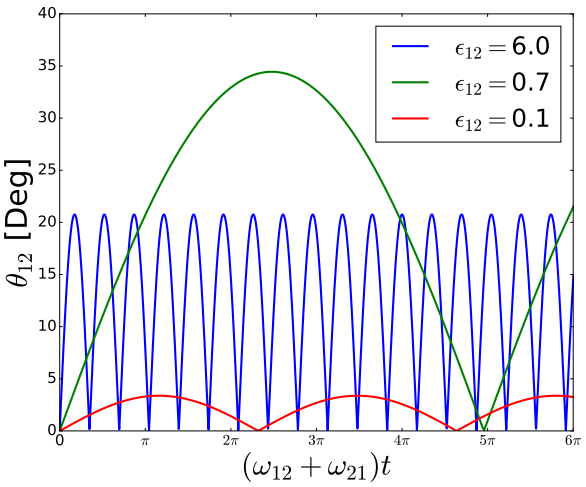

Figure 1. Time evolution of the mutual inclination angle between two inner planets in the presence of an external inclined perturber (at $\theta_p = 10^\circ$). The two planets have mass ratio $m_2/m_1 = 10$, with $a_1 = 0.3$ au, $a_2 = 0.5$ au and are initially aligned. Different curves are for different values of ϵ_{12}, corresponding to different strengths of the perturber (m_p/a_p^3). For $\epsilon_{12} \ll 1$, θ_{12} oscillates with the characteristic frequency ($\omega_{12}+\omega_{21}$) (see Eq. 19); for $\epsilon_{12} \gg 1$, the characteristic frequency is $(\Omega_{2p}-\Omega_{1p})\cos\theta_p$ (see Eq. 22); near the resonance ($\epsilon_{12} \sim 1$; see the green curve), the characteristic frequency is much smaller.

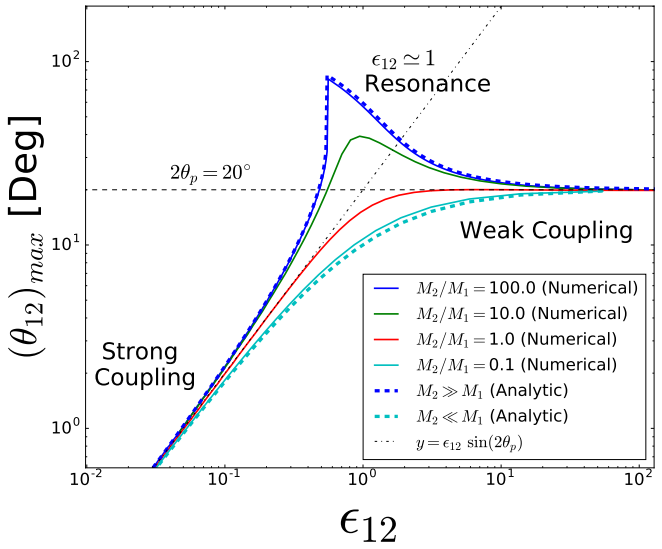

Figure 2. Maximum mutual inclination between two inner planets (m_1, m_2) in the presence of an external perturber (m_p). The inner planets are initially coplanar ($\theta_{12} = 0$) and inclined relative to the perturber at $\theta_p = 10^\circ$. The two planets are located at $a_1 = 0.3$ au and $a_2 = 0.5$ au (but only a_2/a_1 affects the result). The different curves correspond to different mass ratios, as indicated. The dimensionless parameter ϵ_{12} (see Eq. 8 or 12) is varied by varying the "strength" of the perturber, m_p/a_p^3. Analytical results in the strong coupling and weak coupling limits are also shown. A resonance feature is present when $m_2/m_1 \gtrsim 1$.

Here $L_1/L_2 = (m_1/m_2)(a_1/a_2)^{1/2}$ is the ratio of the planet's angular momenta , Ω_{2p}/Ω_{1p} is given by Eq. (7), which simplifies to

$$\frac{\Omega_{2p}}{\Omega_{1p}} \approx \left(\frac{a_2}{a_1}\right)^{3/2} \tag{10}$$

in the quadrupole approximation (valid for $a_p \gg a_2, a_1$), and

$$\hat{\Omega}_{1p} \equiv \frac{\Omega_{1p}}{\omega_{12}} = \frac{m_p}{m_2}\frac{a_2^2\, b_{3/2}^{(1)}(a_1/a_p)}{a_p^2\, b_{3/2}^{(1)}(a_1/a_2)} \approx \frac{m_p}{m_2}\left(\frac{a_2}{a_p}\right)^3 \frac{3a_1/a_2}{b_{3/2}^{(1)}(a_1/a_2)}, \tag{11}$$

where the last equality assumes $a_p \gg a_1$. Thus

$$\epsilon_{12} \approx \left(\frac{m_p}{10^3 m_2}\right)\left(\frac{10a_2}{a_p}\right)^3 \left[\frac{3a_1/a_2}{b_{3/2}^{(1)}(a_1/a_2)}\right] \frac{(a_2/a_1)^{3/2}-1}{1+(L_1/L_2)}. \tag{12}$$

For given inner planet parameters ($m_{1,2}$ and $a_{1,2}$ – in fact, only the ratios m_2/m_1 and a_2/a_1 matter), the result for $(\theta_{12})_{\rm max}$ depends on θ_p and on m_p and a_p through the combination m_p/a_p^3 (for $a_p \gg a_1, a_2$).

In the following subsections we discuss the the behaviors of $(\theta_{12})_{\rm max}$ in the limits of $\epsilon_{12} \ll 1$ (strong coupling) and $\epsilon_{12} \gg 1$ (weak coupling), and as well as the resonance feature around $\epsilon_{12} \sim 1$.

2.2. *Strong Coupling Limit:* $\epsilon_{12} \ll 1$

In the *strong coupling limit*, with $\epsilon_{12} \ll 1$ (see Eq. 8), we expect $\hat{\boldsymbol{l}}_1$ and $\hat{\boldsymbol{l}}_2$ to stay close to alignment. Let $\boldsymbol{L} = \boldsymbol{L}_1 + \boldsymbol{L}_2 \equiv L\hat{\boldsymbol{l}}$ be the total angular momentum of the two inner planets, with $L \simeq L_1 + L_2$. From Eqs. (1)-(2), we find

$$\frac{{\rm d}\hat{\boldsymbol{l}}}{{\rm d}t} \simeq \Omega_L(\hat{\boldsymbol{l}}\cdot\hat{\boldsymbol{l}}_p)(\hat{\boldsymbol{l}}\times\hat{\boldsymbol{l}}_p), \tag{13}$$

where $-\Omega_L(\hat{\boldsymbol{l}}\cdot\hat{\boldsymbol{l}}_p)$ is the precession rate of $\hat{\boldsymbol{l}}$ around $\hat{\boldsymbol{l}}_p$, with

$$\Omega_L \simeq \frac{L_1\Omega_{1p} + L_2\Omega_{2p}}{L_1+L_2}. \tag{14}$$

In the frame corotating with $\hat{\boldsymbol{l}}$, we have

$$\left(\frac{{\rm d}\hat{\boldsymbol{l}}_1}{{\rm d}t}\right)_{\rm rot} = \frac{{\rm d}\hat{\boldsymbol{l}}_1}{{\rm d}t} + \Omega_L(\hat{\boldsymbol{l}}\cdot\hat{\boldsymbol{l}}_p)(\hat{\boldsymbol{l}}_p\times\hat{\boldsymbol{l}}_1) \simeq \left[\Big(\Omega_L\hat{\boldsymbol{l}}\cdot\hat{\boldsymbol{l}}_p - \Omega_{1p}\hat{\boldsymbol{l}}_1\cdot\hat{\boldsymbol{l}}_p\Big)\hat{\boldsymbol{l}}_p - \omega_{12}(\hat{\boldsymbol{l}}_1\cdot\hat{\boldsymbol{l}}_2)\hat{\boldsymbol{l}}_2\right]\times\hat{\boldsymbol{l}}_1. \tag{15}$$

Let $\hat{\boldsymbol{l}}_{1,2} = \hat{\boldsymbol{l}} + \Delta\boldsymbol{l}_{1,2}$, with $|\Delta\boldsymbol{l}_{1,2}| \sim \epsilon_{12} \ll 1$. Note that

$$L_1\Delta\boldsymbol{l}_1 + L_2\Delta\boldsymbol{l}_2 \simeq 0. \tag{16}$$

Equation (15) then becomes, to leading order in ϵ_{12},

$$\left(\frac{{\rm d}\Delta\boldsymbol{l}_1}{{\rm d}t}\right)_{\rm rot} \simeq -(\omega_{12}+\omega_{21})\hat{\boldsymbol{l}}\times\Delta\boldsymbol{l}_1 + (\Omega_{1p}-\Omega_L)(\hat{\boldsymbol{l}}\cdot\hat{\boldsymbol{l}}_p)(\hat{\boldsymbol{l}}\times\hat{\boldsymbol{l}}_p), \tag{17}$$

For $\Delta\boldsymbol{l}_1(t=0) = 0$, the leading-order solution is

$$\Delta\boldsymbol{l}_1(t) \simeq \frac{L_2}{L}\epsilon_{12}\cos\theta_p\Big[(1-\cos\tau_{12})(\hat{\boldsymbol{l}}_p\times\hat{\boldsymbol{l}})\times\hat{\boldsymbol{l}} + \sin\tau_{12}\,(\hat{\boldsymbol{l}}_p\times\hat{\boldsymbol{l}})\Big], \tag{18}$$

where we have used $\hat{\boldsymbol{l}}\cdot\hat{\boldsymbol{l}}_p = \cos\theta_p$ and $\tau_{12} \equiv (\omega_{12}+\omega_{21})t$. Using Eqs. (18) and (16), we then find that the mutual inclination angle θ_{12} between $\hat{\boldsymbol{l}}_1$ and $\hat{\boldsymbol{l}}_2$ is given by

$$|\sin\theta_{12}| = \left|\hat{\boldsymbol{l}}_1\times\hat{\boldsymbol{l}}_2\right| \simeq \epsilon_{12}\left|\sin 2\theta_p \sin\frac{\tau_{12}}{2}\right|. \tag{19}$$

Thus, the maximum and the RMS values of $|\sin\theta_{12}|$ are

$$|\sin\theta_{12}|_{\rm max} \simeq \epsilon_{12}\,|\sin 2\theta_p|\,, \tag{20}$$

$$\left\langle\sin^2\theta_{12}\right\rangle^{1/2} \simeq \frac{1}{\sqrt{2}}\epsilon_{12}\,|\sin 2\theta_p|\,. \tag{21}$$

2.3. *Weak Coupling Limit:* $\epsilon_{12} \gg 1$

In the *weak coupling limit*, with $\epsilon_{12} \gg 1$, the vectors $\hat{\boldsymbol{l}}_1$ and $\hat{\boldsymbol{l}}_2$ precess around $\hat{\boldsymbol{l}}_p$ independently, with constant $\hat{\boldsymbol{l}}_1\cdot\hat{\boldsymbol{l}}_p \simeq \hat{\boldsymbol{l}}_2\cdot\hat{\boldsymbol{l}}_p \simeq \cos\theta_p$. Thus

$$\left|\hat{\boldsymbol{l}}_1\times\hat{\boldsymbol{l}}_2\right|^2 \simeq \sin^2 2\theta_p\,\sin^2\Big(\frac{\Delta\phi_{12}}{2}\Big) + \sin^4\theta_p\,\sin^2(\Delta\phi_{12}), \tag{22}$$

where $\Delta\phi_{12} \simeq (\Omega_{2p}-\Omega_{1p})(\cos\theta_p)t$. The maximum of θ_{12} and the RMS value of $|\sin\theta_{12}|$ are

$$(\theta_{12})_{\rm max} \simeq 2\theta_p, \tag{23}$$

$$\left\langle\sin^2\theta_{12}\right\rangle^{1/2} \simeq \frac{1}{\sqrt{2}}\left(\sin^2 2\theta_p + \sin^4\theta_p\right)^{1/2}. \tag{24}$$

2.4. *Resonance*

Figure 2 reveals that when $m_2 \gtrsim m_1$ (i.e., the outer planet is more massive than the inner planet), a resonance feature appears around $\epsilon_{12} \sim 1$. At the resonance, $(\theta_{12})_{\rm max}$ can become much larger than the weak-coupling limit, $2\theta_p$. When $m_1 \gtrsim m_2$, no resonance feature exists.

This resonance feature can be understood analytically in the limit when the planetary system contains a "dominant" planet (labeled "d") which is much more massive than the other planet (labeled "j"), i.e., $m_d \gg m_j$. In Appendix A we develop the Hamiltonian theory for such systems. We show that for $\theta_p \ll 1$, a sharp resonance appears at $|\epsilon_{jd}| = 1$, or

$$\Omega_{dp} = \Omega_{jp} + \omega_{jd}, \quad \Big(\text{resonance for } \frac{m_d}{m_j} \gg 1,\ \theta_p \ll 1\Big). \tag{25}$$

This resonance condition is easy to interpret physically: The dominant planet experiences nodal precession at the frequency Ω_{dp} driven by the perturber, while the subdominant planet m_j precesses at the rate $(\Omega_{jp}+\omega_{jd})$ driven by both the perturber and the dominant planet; resonance occurs when these two precession frequencies match[4]. Clearly, to satisfy Eq. (25) requires $\Omega_{dp} > \Omega_{jp}$,

[4] The resonance can also be "visualized" geometrically (see

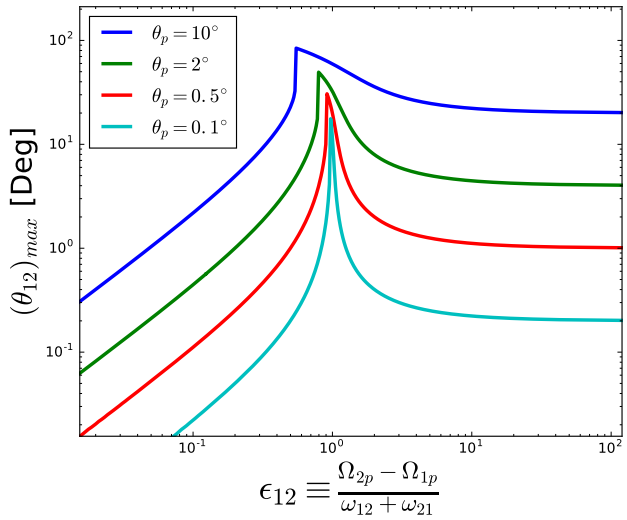

Figure 3. Maximum misalignment angle between two inner planets in the presence of an external perturber, as a function of ϵ_{12}, in the limit of $m_2 \gg m_1$. Note that in this limit, $\omega_{21} = (L_1/L_2)\omega_{12} \ll \omega_{12}$. The two planets are located at $a_1 = 0.3$ au and $a_2 = 0.5$ au. Different curves correspond to different inclination angles (θ_p) of the external perturber. These curves are obtained analytically by solving Eq. (A8) derived in Appendix A. The resonant feature is most prominent for $\theta_p \ll 1$ and is located at $\epsilon_{12} = 1$ in the $\theta_p \to 0$ limit. As θ_p increases, the resonance feature is broadened and shifted to slightly smaller ϵ_{12}.

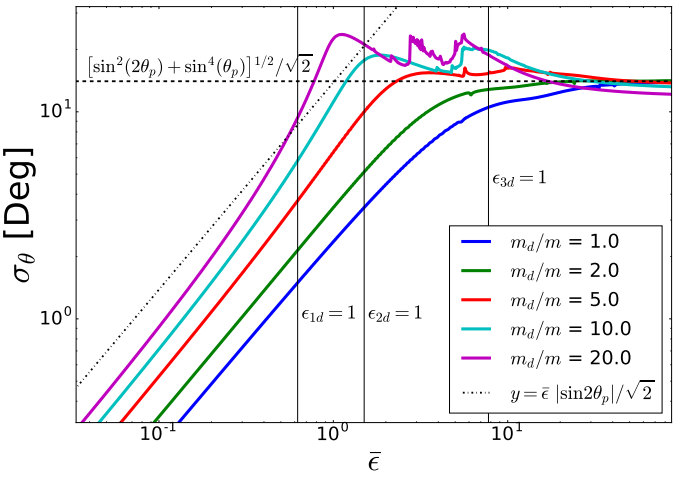

Figure 4. Spread in mutual inclination σ_θ (defined by Eqs. 27-28) between four planets in the presence of an external perturber (m_p) as a function of the coupling parameter $\bar{\epsilon}$ (defined by Eq. 29). The four planets are located at the semi-major axes 0.1, 0.15, 0.25, 0.4 au, and are initially coplanar and inclined relative to the perturber at $\theta_p = 10^\circ$. The dominant planet (the one with the largest mass, m_d) is the 4th planet (with the largest semi-major axis), and the other three planets have the same mass $m_j = m$. The different curves correspond to different mass ratio m_d/m, as indicated. The dimensionless parameter $\bar{\epsilon}$ is varied by varying the "strength" of the perturber, m_p/a_p^3. Analytical results in the strong coupling limit (Eq. 34) and weak coupling limit (Eq. 36), derived under the assumption $m_d/m \gg 1$, are also shown. Three resonance features are present when m_d/m is sufficiently large. In the limit of $m_d/m \gg 1$ and $\theta_p \to 0$, these resonances are located at $\epsilon_{1d} = 1$, $\epsilon_{2d} = 1$ and $\epsilon_{3d} = 1$.

or $a_d > a_j$, i.e., the dominant planet exterior to the subdominant planet. Near the resonance, the maximum mutual inclination behaves as (see Appendix A)

$$(\theta_{jd})_{\max} \simeq \frac{2\epsilon_{jd}\theta_p}{|\epsilon_{jd} - 1|} \tag{26}$$

(valid for general ϵ_{jd} but $\theta_p, \theta_{jd,\max} \ll 1$). This provides an estimate for the "width" of the resonance for $\theta_p \ll 1$).. As θ_p increases, the resonance becomes broader and is shifted slightly to smaller ϵ_{12} (see Fig. 3). Also, as the mass ratio m_d/m_j decreases, the resonance feature gradually become "smoothed" out and disappears when $m_d/m_j \lesssim 1$ (see Fig. 2).

3. MULTI-PLANET SYSTEMS WITH EXTERNAL PERTURBER

The evolution equations for the orientations of multi-planet ($N > 2$) systems with an external perturber can be easily can be generalized (see Appendix B). Figures 4-6 show some numerical results for a 4-planet system ($N = 4$) in the presence of an external perturber. To characterize the mutual misalignment of the planets for a wide range of parameters, we take the dominant planet (the one with the largest mass, labeled "d") in the system and measure the relative inclination ($\hat{\boldsymbol{l}}_j$) of the other planets with respect to $\hat{\boldsymbol{l}}_d$. We define the RMS of $|\hat{\boldsymbol{l}}_j \times \hat{\boldsymbol{l}}_d|$ as

$$\mathrm{RMS}\,(\sin\Delta\theta) \equiv \left(\frac{1}{N-1} \left\langle \sum_{j \neq d} |\hat{\boldsymbol{l}}_j \times \hat{\boldsymbol{l}}_d|^2 \right\rangle \right)^{1/2}, \tag{27}$$

and the mutual inclination spread as

$$\sigma_\theta \equiv \sin^{-1}\Big[\mathrm{RMS}\,(\sin\Delta\theta)\Big]. \tag{28}$$

We also define the averaged coupling parameter of the system as

$$\bar{\epsilon} \equiv \left(\frac{1}{N-1} \sum_{j \neq d} |\epsilon_{jd}|^2 \right)^{1/2}. \tag{29}$$

Other ways of characterizing mutual inclinations are possible (see Appendix B), but Eqs. (27) and 29 allow for simple analytical expressions in the limiting cases, as we discuss below.

To understand the numerical results shown in Fig. 4-6, we consider the limiting case of $m_d \gg m_j$ (with $j \neq$

Fig. 2 in Lai 2014) by considering Eq. (15) with $1 \to j$, $2 \to d$, $\hat{\boldsymbol{l}} \to \hat{\boldsymbol{l}}_d$ and $\Omega_L \to \Omega_{dp}$: When $\hat{\boldsymbol{l}}_p$, $\hat{\boldsymbol{l}}_d$ and $\hat{\boldsymbol{l}}_j$ are approximately aligned, and when the system is near resonance, $\hat{\boldsymbol{l}}_1$ precesses around the vector $(\hat{\boldsymbol{l}}_p - \hat{\boldsymbol{l}}_d)$, which is almost perpendicular to $\hat{\boldsymbol{l}}_1$, thus producing a large θ_{jd}.

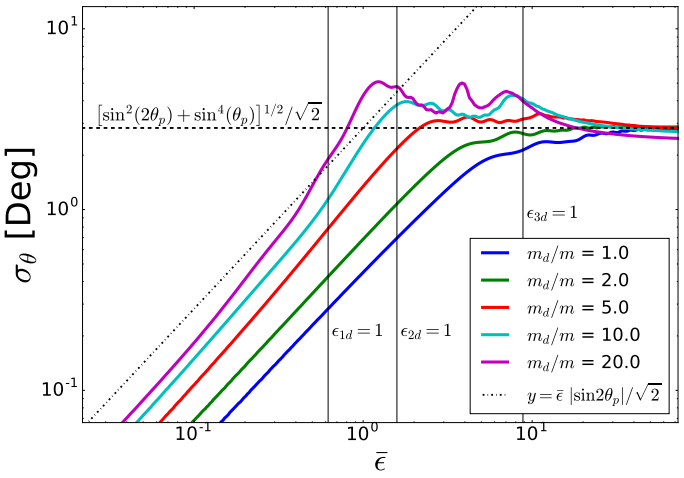

Figure 5. Same as Fig. 4, except for $\theta_p = 2°$.

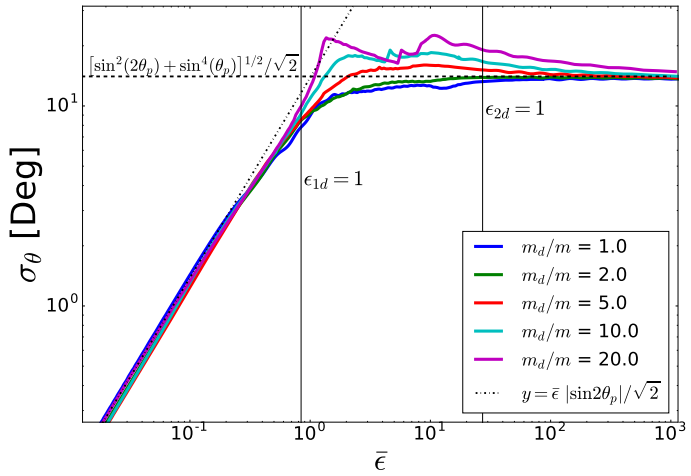

Figure 6. Same as Fig. 4, except that the third planet is the dominant planet.

d). The angular momentum axis of the dominant planet precesses around $\hat{\boldsymbol{l}}_p$ with an approximately constant $\hat{\boldsymbol{l}}_d \cdot \hat{\boldsymbol{l}}_p = \cos\theta_p$. The sub-dominant planets are "shepherded" by m_d in addition to the external perturber m_p.

In the *strong coupling limit*, with $|\epsilon_{jd}| \ll 1$, where

$$\epsilon_{jd} \equiv \frac{\Omega_{dp} - \Omega_{jp}}{\omega_{jd} + \omega_{dj}}, \tag{30}$$

we have (cf. Eq. 18)

$$\hat{\boldsymbol{l}}_j - \hat{\boldsymbol{l}}_d \simeq \epsilon_{jd}\cos\theta_p \Big[(1-\cos\tau_{jd})(\hat{\boldsymbol{l}}_p\times\hat{\boldsymbol{l}}_d)\times\hat{\boldsymbol{l}}_d + \sin\tau_{jd}\,(\hat{\boldsymbol{l}}_p\times\hat{\boldsymbol{l}}_d)\Big], \tag{31}$$

where $\tau_{jd} \equiv (\omega_{jd}+\omega_{dj})t$. Thus

$$|\sin\theta_{jd}| = \left|\hat{\boldsymbol{l}}_j \times \hat{\boldsymbol{l}}_d\right| \simeq \left|\epsilon_{jd}\sin 2\theta_p \sin\frac{\tau_{jd}}{2}\right|. \tag{32}$$

The misalignment spread of the N planets is measured by

$$\frac{1}{N-1}\Big\langle\sum_j |\hat{\boldsymbol{l}}_j\times\hat{\boldsymbol{l}}_d|^2\Big\rangle \simeq \frac{1}{2(N-1)}\Big(\sum_j |\epsilon_{jd}|^2\Big)\sin^2 2\theta_p, \tag{33}$$

i.e.,

$$\mathrm{RMS}\,(\sin\Delta\theta) \simeq \frac{1}{\sqrt{2}}\,\bar{\epsilon}\,|\sin 2\theta_p|\,. \tag{34}$$

From Eq. (31), we also find

$$\langle\sin^2\theta_{jk}\rangle = \Big\langle|\hat{\boldsymbol{l}}_j\times\hat{\boldsymbol{l}}_k|^2\Big\rangle \simeq \frac{\sin^2 2\theta_p}{2}\left(\epsilon_{jd}^2+\epsilon_{kd}^2-\epsilon_{jd}\epsilon_{kd}\right). \tag{35}$$

In Appendix B we present a more rigorous way to characterize the mutual inclination and the exact analytical expression in the strong coupling limit.

In the *weak coupling limit*, with $|\epsilon_{jd}| \gg 1$, all $\hat{\boldsymbol{l}}_j$'s precess independently around $\hat{\boldsymbol{l}}_p$. We have

$$\mathrm{RMS}\,(\sin\Delta\theta) \simeq \frac{1}{\sqrt{2}}\left(\sin^2 2\theta_p + \sin^4\theta_p\right)^{1/2}, \tag{36}$$

and

$$\langle\sin^2\theta_{jk}\rangle^{1/2} \simeq \frac{1}{\sqrt{2}}\left(\sin^2 2\theta_p + \sin^4\theta_p\right)^{1/2}. \tag{37}$$

Figures 4-reffig6 show that the numerical results match the analytical expressions in both strong and weak coupling limits. [5] Resonance features also occur whenever a "minor" planet exists inside the dominant planet. The resonance is located at $\epsilon_{jd} \sim 1$ (with $a_j < a_d$).

Note that the small-scale non-smooth features seen in Figs. 4-6 are real, and likely result from the chaotic behavior the system due to the overlap of multiple nonlinear resonances. We will study this and other related issues in a future paper.

4. SUMMARY AND DISCUSSION

4.1. *Key Results*

We have calculated the excitation of mutual inclinations in compact planetary systems by external planetary or stellar companions. Our key results are summarized in Figs. 2-6 and a number of approximate analytic expressions can be used to assess the importance of external perturbers of various masses (m_p), semi-major axis (a_p) and inclination (θ_p). In general, the mutual inclination excited by a perturber depends on the dimensionless coupling parameter ϵ_{12} (Eq. 8 or 30), which measures the ratio of the differential precession rate of

[5] Note that in the strong-coupling regime, the agreement between the numerical result and the analytical expression is much better in Fig. 6 than in Figs. 4 and 5. The reason is that putting the dominant planet in the middle of the system makes it more "dominant" because of its stronger coupling with the other inner planets, whereas placing the dominant planet at the edge of the inner system makes it not as dominant in terms of mutual couplings (i.e. some of the farther planets may have comparable coupling to each other compared to the "dominant" planet in this case).

planet 1 and 2 induced by the perturber and their mutual precession rate. In order of magnitude, we have (Eq. 12)

$$\epsilon_{12} \sim \left(\frac{m_p}{m_2}\right)\left(\frac{a_2}{a_p}\right)^3, \quad (38)$$

for $m_2 \sim m_1$ and $a_2 \gtrsim a_1$.

For a two-planet system (see Fig. 2), the mutual inclination induced by an external companion is comparable to θ_p when $\epsilon_{12} \gtrsim 1$ (see Eqs. 23-24), but becomes $\sim \epsilon_{12}\theta_p$ when $\epsilon_{12} \lesssim 1$ (see Eqs. 20-21). However, when $m_2 \gtrsim 2m_1$ (i.e., the exterior planet is more massive), a resonance feature appears at around $\epsilon_{12} \sim 1$ where the mutual inclination may greatly exceed θ_p (see Fig. 3). This enhanced inclination excitation is the resulr of a secular nodal precession resonance (Appendix A).

The excitation of mutual inclinations in systems with more planets is necessarily more complex (Section 3 and Appendix B). Nevertheless, qualitative similar results can be obtained when the mutual inclination is measured relative to the more massive ("dominant") planet in the system and when an averaged coupling parameter $\bar{\epsilon}$ is introduced (Eq. 29). Indeed, our approximate analytic expressions for the mutual inclination spread (Eq. 34 in the strong coupling limit and Eq. 36 in the weak coupling limit) are in agreement with the numerical results (see Figs. 4-6).

4.2. *Applications to Individual Systems*

As noted in Section 1, a number of "inner planets + companion" systems have been observed. Here we discuss some of these systems in light of our theoretical results.

Kepler-68 ($M_\star = 1.08M_\odot$, $R_\star = 1.24R_\odot$) has two transiting planets ($m_{1,2} = 8.3,\ 4.8M_\oplus$) at $a_{1,2} = 0.0617,\ 0.0906$ au, and a non-transiting giant planet $m_p \gtrsim 0.95M_J$ at $a_p = 1.4$ au ($e_p = 0.18$) (Gilliland et al. 2013). The coupling parameter is $\epsilon_{12} \simeq 2.3 \times 10^{-3}$ using the lower limit for m_p. The excited mutual inclination spread of the two inner planet is $\sigma_\theta = \epsilon_{12} \sin 2\theta_p/\sqrt{2} \lesssim 0.14^\circ$ (regardless of θ_p), and is smaller than $R_\star/a_2 = 3.6^\circ$, consistent with the coplanarity of the two inner planets.

Kepler-48 ($M_\star = 0.88M_\odot$, $R_\star = 0.89R_\odot$) has three transiting inner planets ($m_{1,2,3} = 0.0124, 0.046, 0.015M_J$) at $a_{1,2,3} = 0.053, 0.085, 0.23$ au, and a giant planet ($m_p \gtrsim 2.1M_J$) at $a_p = 1.85$ au (982 days) (Marcy et al. 2014). The coupling parameters are $\epsilon_{12} \simeq 0.0015$ and $\epsilon_{23} \simeq 0.25$ using $m_p = 2.1M_J$. Significant mutual inclination can be excited between planet 2 and 3 if θ_p is large. Requiring $\theta_{23} \sim \epsilon_{23}\theta_p \lesssim R_\star/a_3 = 1.03^\circ$ yields $\theta_p \lesssim 2.3^\circ$. We therefore predict that the non-transiting planet (Kepler-48e) is closely aligned with the inner transiting planets. Note that since $R_\star/a_p = 0.13^\circ$, its transit probability is still small.

Kepler-56 (with a red giant host star $M_\star = 1.32M_\odot$, $R_\star = 4.23R_\odot$) has two transiting planets ($m_{1,2} = 0.0695, 0.57M_J$) at $a_{1,2} = 0.103, 0.165$ au (period 10.5, 21 days). The orbits of the two planets are coplanar within $\sim R_\star/a_2 = 6.8^\circ$, and are inclined with respect to the stellar equator by more than 37° (Huber et al. 2013). RV observations reveal a third planet with period 1002 days ($a_p = 2.16$ au), $e_p = 0.2$, and $m_p \geq 5.6M_J$ (Oter et al. 2016). This implies a coupling parameter of $\epsilon_{12} \geq 1.6 \times 10^{-3}$. Thus the inner two planets are strongly coupled and their coplanarity is not affected by any (regardless of θ_p) external perturbers that satisfy the current RV constraint. However, the observed large stellar obliquity may require a large θ_p.

WASP-47 ($M_\star = 1.04M_\odot$) contains three transiting planets (Becker et al. 2015; Dai et al. 2015): a hot Jupiter ($1.16M_J$, $a_2 = 0.051$ au or 4.16 days) with an inner super-Earth ($1.8R_\oplus$ or $12M_\oplus$, 0.79 days) and an outer Neptune-size planet ($3.6R_\oplus$ or $10.4 \pm 8.4M_\oplus$, 9.03 days). These inner planets are orbited by an external giant planet ($m_p > 1.24M_J$) with $e = 0.13$ and $P = 572$ days (Neveu-VanMalle et al. 2016). The inner planets are well in the strong coupling regime, with $|\epsilon_{jk}| \ll 1$ ($\epsilon_{12} = 2 \times 10^{-4}$ and $\epsilon_{23} = 1.7 \times 10^{-4}$).

Kepler-454 ($M_\star = 1.03M_\odot$) has a 10.6 day ($a_1 = 0.095$ au) transiting planet ($2.37R_E$, $6.84M_\oplus$), a cold Jupiter ($m_p > 4.46M_J$ at 524 days) and a distant companion ($>12M_J$ at >10 years) (Gettel et al. 2016). The observed system has $\epsilon = (m_p/m_1)(a_1/a_p)^3 \sim 0.1(m_p/5M_J)$. A neighboring planet $m_2 \sim m_1$ would give $\epsilon_{12} \sim (a_2/0.2\ \text{au})^3(m_p/5M_J)$, and would be easily inclined relative to m_1 and not observable. Thus Kepler-454 could be an example of multi-planet systems that haven been "disrupted" by giant planet perturbers.

GJ 832 ($M_\star = 0.832M_\odot$) has a super Earth ($m_1 > 5.4M_\oplus$ at 0.162 au) inside a giant planet ($m_p > 0.64M_J$ at 3.4 au), both discovered by RV (Wittenmyer et al. 2014). With $\epsilon = (m_p/m_1)(a_1/a_p)^3 \sim 0.006(m_p/M_J)(m_1/6M_\oplus)^{-1}$, any neighboring planet to m_1 is strongly coupled to it.

55 Cancri ($M_\star = 0.95M_\odot$) has four inner planets (e,b,c,f) with $m_{e,b} \simeq 0.027,\ 0.83M_J$, $m_c > 0.17M_J$, $m_f > 0.16M_J$ at 0.0156, 0.115, 0.24, 0.78 au, and an external giant planet (d) with $m_d > 3.8M_J$ and $a_d = 5.74$ au (Dawson & Fabrycky 2010). The outer planet may be inclined with respect to the line of sight by $\sim 53^\circ$ (McArthur et al. 2004), implying $\theta_p \gtrsim 37^\circ$ relative to planet e. Since $\epsilon = (m_d/m_f)(a_f/a_d)^3 \sim 0.08(m_d/5M_J)(m_f/0.16M_J)^{-1}$, planet d, even if highly misaligned, cannot significantly influence the coplanarity of the inner planets. The planetary system is also orbited by a distant stellar companion 55 Cnc B at $a_B \sim 1065$ au (projected distance). But this will not perturb the coplanarity of the planets since $(M_B/m_d)(a_d/a_B)^3 \ll 1$.

Kepler-444 ($M_\star = 0.76M_\odot$) has five sub-Earth radius planets (0.40 - $0.74R_\oplus$) at semi-major axes 0.0418, 0.0488, 0.06, 0.0696, 0.0811 au (Campante et al. 2015) orbiting the primary star (Kepler-444A). Astrometric and RV observations show that a pair of M dwarfs (BC) with total mass $m_p \equiv m_{BC} = 0.54M_\odot$

orbits around Kepler-444A with semi-major axis $a_p \simeq 37$ au and eccentricity $e_p = 0.864$ (Dupuy et al. 2016). Both the planetary system and the A-BC binary have edge-on orbits relative to the line of sight. Using $m_5 \sim 0.54 M_\oplus$ [from the planet mass-radius relation $m/M_\oplus \simeq (R/R_\oplus)^{2.06}$], we find the coupling parameter $\epsilon \sim (m_{BC}/m_5)\left(a_5/a_p\sqrt{1-e_p^2}\right)^3 \sim 0.026$, and thus the five planets are strongly coupled and can maintain their coplanarity (in agreement with the numerical simulation of Dupuy et al. 2016).

4.3. *Implications for Kepler Dichotomy*

The common occurrence of giant planets and stellar companions outside compact planetary systems (see Sections 1 and 4.2) suggests that these giant planets or more massive distant stellar perturbers can excite mutual inclinations in the inner planets, thereby account for an appreciable fraction of the Kepler "singles". Our work provides a quantitative criterion (in terms of the strength of the perturber, m_p/a_p^3) for inclination excitations. Continued search for external companions of inner transiting planets would help constrain various scenarios (see Section 1) for producing the Kepler dichotomy.

As noted in Section 1, inclined stellar companions may be a natural consequence of the binary formation process, while inclined giant planets may be produced by strong planet-planet scatterings. In the latter case, the inner multi-planet system may experience some excitation of mutual inclinations while the outer giant planets undergo scatterings. (Of course, if the inner planets are not well separated from the outer giants, they may be completely disrupted.) Our numerical calculations (Pu & Lai 2016, in prep) suggest that in many cases, the mutual inclination excitation in the inner system during the outer-planet scattering phase is smaller than the subsequent secular phase.

In this paper we have focused on the excitation of mutual inclinations, since they most directly influence the transit probability of multiple planets. Eccentricities are also excited by external companions (Pu & Lai 2016, in prep). This may explain why Kepler "singles" (or a fraction of them) are more eccentric than the Kepler "multis", for which the exists tentative observational evidence (J. Xie et al. 2016).

While Kepler single-transit systems may contain other planets hidden from transit observations due to mutual inclinations, it is also possible that they are true "singles" because of the dynamical influences of external giant planets. For example, when appreciable mutual inclinations and eccentricities are excited, the inner planetary systems are likely more unstable and will suffer self-destruction (e.g. Veras & Armitage 2004; Pu & Wu 2015). In addition, as noted above, the inner planetary systems could have been severely disrupted while strong planet scatterings took place at a few au's that produced inclined/eccentric giant planets. Continued search for close neighbors of single-transit planets would shed light on this issue.

ACKNOWLEDGMENTS

This work has been supported in part by NSF grant AST-1211061, NASA grants NNX14AG94G and NNX14AP31G, and a Simons Fellowship to DL from the Simons Foundation.

APPENDIX

A. HAMILTONIAN THEORY FOR RESONANCE

We consider a system with a "dominant" planet (labeled "d") whose mass and angular momentum are much larger than the other planets ($m_d \gg m_j$ and $L_d \gg L_j$, with $j \neq d$). The Hamiltonian governing the dynamics of $\hat{\boldsymbol{l}}_j(t)$ is

$$H = -\frac{1}{2}\,\omega_{jd}\,L_j\,(\hat{\boldsymbol{l}}_j\cdot\hat{\boldsymbol{l}}_d)^2 - \frac{1}{2}\,\Omega_{jp}\,L_j\,(\hat{\boldsymbol{l}}_j\cdot\hat{\boldsymbol{l}}_p)^2, \qquad \text{(A1)}$$

where we have neglected a non-essential additive constant. Since m_d is the dominant planet, its $\hat{\boldsymbol{l}}_d$ simply precesses around $\hat{\boldsymbol{l}}_p$ with a constant rate, $-\Omega_{dp}\,(\hat{\boldsymbol{l}}_d\cdot\hat{\boldsymbol{l}}_p) \simeq -\Omega_{dp}\cos\theta_p$:

$$\frac{\mathrm{d}\hat{\boldsymbol{l}}_d}{\mathrm{d}t} \simeq -\Omega_{dp}(\hat{\boldsymbol{l}}_d\cdot\hat{\boldsymbol{l}}_p)\,\hat{\boldsymbol{l}}_p\times\hat{\boldsymbol{l}}_d. \qquad \text{(A2)}$$

In the frame corotating with $\hat{\boldsymbol{l}}_d$, the Hamiltonian (A1) transforms to

$$H_{\rm rot} \simeq H + \Omega_{dp}\,(\hat{\boldsymbol{l}}_d\cdot\hat{\boldsymbol{l}}_p)\,\hat{\boldsymbol{l}}_p\cdot(L_j\hat{\boldsymbol{l}}_j). \qquad \text{(A3)}$$

It is convenient to use the rescaled Hamiltonian,

$$\tilde{H}_{\rm rot} = \frac{H_{\rm rot}}{L_j} \simeq -\frac{1}{2}\,\omega_{jd}\,\cos^2\theta_{jd} - \frac{1}{2}\,\Omega_{jp}\,(\hat{\boldsymbol{l}}_j\cdot\hat{\boldsymbol{l}}_p)^2 + \Omega_{dp}\cos\theta_p\,(\hat{\boldsymbol{l}}_j\cdot\hat{\boldsymbol{l}}_p), \qquad \text{(A4)}$$

where

$$\hat{\boldsymbol{l}}_j\cdot\hat{\boldsymbol{l}}_p = \sin\theta_p\sin\theta_{jd}\cos\varphi_{jd} + \cos\theta_p\cos\theta_{jd}. \qquad \text{(A5)}$$

Here θ_{jd} and φ_{jd} are the polar angle and azimuthal angle of $\hat{\boldsymbol{l}}_j$ measured relative to $\hat{\boldsymbol{l}}_d$ (i.e., $\cos\theta_{jd} = \hat{\boldsymbol{l}}_j\cdot\hat{\boldsymbol{l}}_d$). Note that φ_{jd} and $\cos\theta_{jd}$ form the conjugate coordinate and momentum for the Hamiltonian $\tilde{H}_{\rm rot}$.

Suppose $\theta_{jd} = 0$ at $t = 0$. Then the phase-space curve for the evolution of $\cos\theta_{jd}$ and φ_{jd} is determined by

$$-\frac{1}{2}\,\hat{\Omega}_{jp}\,(\hat{\boldsymbol{l}}_j\cdot\hat{\boldsymbol{l}}_p)^2 + \hat{\Omega}_{dp}\cos\theta_p\,(\hat{\boldsymbol{l}}_j\cdot\hat{\boldsymbol{l}}_p) + \frac{1}{2}\,\sin^2\theta_{jd} \simeq \left(\hat{\Omega}_{dp} - \frac{1}{2}\hat{\Omega}_{jp}\right)\cos^2\theta_p, \qquad \text{(A6)}$$

where

$$\hat{\Omega}_{jp} \equiv \frac{\Omega_{jp}}{\omega_{jd}}, \quad \hat{\Omega}_{dp} \equiv \frac{\Omega_{dp}}{\omega_{jd}}. \qquad \text{(A7)}$$

The maximum value $\theta_m \equiv (\theta_{jd})_{\rm max}$ is achieved at $\varphi_{jd} = 0$ or π, and is given by

$$-\frac{1}{2}\,\hat{\Omega}_{jp}\,\cos^2(\theta_m \mp \theta_p) + \hat{\Omega}_{dp}\cos\theta_p\,\cos(\theta_m \mp \theta_p) + \frac{1}{2}\,\sin^2\theta_m \simeq \left(\hat{\Omega}_{dp} - \frac{1}{2}\hat{\Omega}_{jp}\right)\cos^2\theta_p, \qquad \text{(A8)}$$

where the upper (lower) sign is for $\varphi_{jd}=0$ (π).

Figures A1 and A2 show some example phase-space curves for the cases of $a_d > a_j$ and $a_d < a_j$, respectively. These two cases have very different phase-space structure, with the former showing clear resonance feature.

Equation (A8) can be solved analytically in several limiting cases:

(i) In the *strong coupling limit* (but general θ_p), $\hat{\Omega}_{jp}, \hat{\Omega}_{dp} \ll 1$, we expect $\theta_m \ll 1$. Expanding Eq. (A8) for small θ_m, we find

$$\theta_m \simeq \mp \epsilon_{jd} \sin 2\theta_p, \qquad \text{i.e.,} \quad \theta_m \simeq |\epsilon_{jd} \sin 2\theta_p|, \tag{A9}$$

in agreement with Eq. (20).

(ii) In the *weak coupling limit* (but general θ_p), $\hat{\Omega}_{jp}, \hat{\Omega}_{dp} \gg 1$, Eq. (A8) has the solution (see Eq. 23)

$$\theta_m \simeq 2\theta_p \qquad (\text{with} \quad \varphi_{jd}=0). \tag{A10}$$

(iii) In *the singular limit of* $\theta_p = 0$, Eq. (A8) has two roots: The first root is $\theta_m = 0$. The second root is

$$\cos\theta_m = \frac{2\hat{\Omega}_{dp}}{1+\hat{\Omega}_{jp}} - 1, \qquad (\text{2nd root}) \tag{A11}$$

which exists only when $|\cos\theta_m| < 1$, or $\epsilon_{jd} = \hat{\Omega}_{dp} - \hat{\Omega}_{jp} < 1$.

(iv) In the limit of $\theta_p \ll 1$ (but general ϵ_{jd}), the second root (Eq. A11) remains valid provided that $\theta_m \gg \theta_p$:

$$\cos\theta_m \simeq \frac{2\hat{\Omega}_{dp}}{1+\hat{\Omega}_{jp}} - 1, \qquad (\text{2nd root; valid for } \theta_m \gg \theta_p) \tag{A12}$$

This root (which exists only when $\epsilon_{jd} = \hat{\Omega}_{dp} - \hat{\Omega}_{jp} \lesssim 1$) cannot be reached for systems with initially aligned inner planets ($\theta_{jd}=0$) (see Figs. A1 and A2). The correction to the first root ($\theta_m = 0$ in the limit of $\theta_p = 0$) due to finite (but small) θ_p can be obtained by expanding Eq. (A8) for $\theta_p, \theta_m \ll 1$. We find

$$\theta_m \simeq \pm \frac{2\epsilon_{jd}\theta_p}{\epsilon_{jd}-1} \qquad (\text{for general } \epsilon_{dj}, \text{ but } \theta_p, \theta_m \ll 1) \tag{A13}$$

(recall that the upper/lower sign is for $\varphi_{jd}=0,\pi$). Clearly, Eq. (A13) reduces to (A9) and (A10) in the appropriate limits. Most importantly, Eq. (A13) shows that a sharp resonance occurs when

$$\epsilon_{jd} = \frac{\Omega_{dp}-\Omega_{jp}}{\omega_{jd}} = 1. \tag{A14}$$

At the resonance, $\theta_m \gg \theta_p$ can be attained (but note that Eq. A13 breaks down for $\epsilon_{jd} \to 1$). Clearly, the resonance condition can be realized only if $a_d > a_j$ (i.e, the dominant planet is outside the "minor" one). Note that Eq. (A14) is exact only in the limit of $\theta_p \to 0$ and $m_d \gg m_j$; otherwise the resonance is shifted and broadened (see Figs. 2-6).

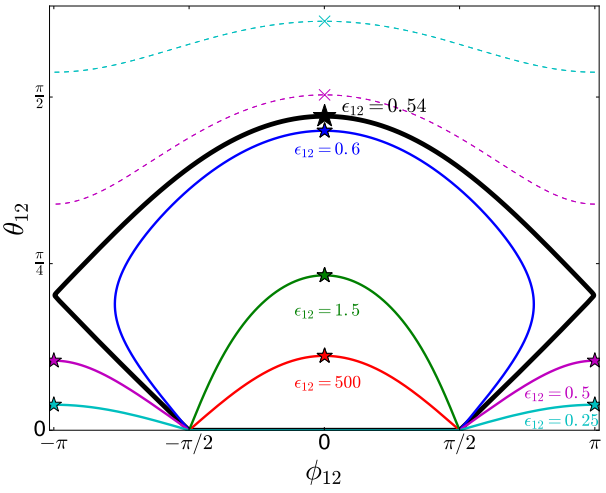

Figure A1. Phase-space curves for the mutual inclination of a two-planet system with an external perturber. The two planets have $a_1 = 0.3$ au and $a_2 = 0.5$ au, with masses $m_2 \gg m_1$, and the perturber's orbit is inclined at $\theta_p = 10°$. The different curves correspond to different values of ϵ_{12}, as indicated; the solid curves can be reached by an initially aligned system ($\theta_{12}=0$), while the dashed curves are unreachable. The maximum θ_{12} for each value of ϵ_{12} is marked. The thick solid line is the separatrix (corresponding to a critical value of ϵ_{12}) at which (θ_{12})max experiences a sudden jump (see Fig. 3).

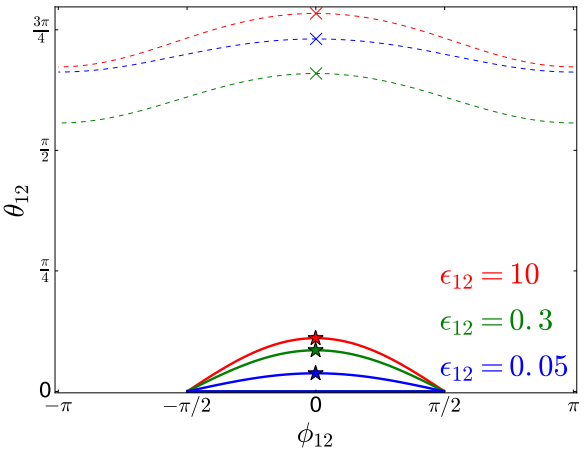

Figure A2. Same as Fig. A1 except for $m_2 \ll m_1$.

B. GENERAL EQUATIONS FOR MULTI-PLANET SYSTEMS

The result of Section 2 can be easily generalized to a system with N inner planets with an inclined external perturber m_p. The evolution of $\hat{\boldsymbol{l}}_j$ ($j=1,2,\cdots,N$) is governed by the equation

$$\frac{d\hat{\boldsymbol{l}}_j}{dt} = \sum_{k\neq j} \omega_{jk}(\hat{\boldsymbol{l}}_j\cdot\hat{\boldsymbol{l}}_k)(\hat{\boldsymbol{l}}_j\times\hat{\boldsymbol{l}}_k) + \Omega_{jp}(\hat{\boldsymbol{l}}_j\cdot\hat{\boldsymbol{l}}_p)(\hat{\boldsymbol{l}}_j\times\hat{\boldsymbol{l}}_p), \tag{B15}$$

where

$$\omega_{jk} = \frac{Gm_j m_k a_<}{4a_>^2 L_j} b_{3/2}^{(1)}\left(\frac{a_<}{a_>}\right), \tag{B16}$$

$$\Omega_{jp} = \frac{Gm_j m_p a_j}{4a_p^2 L_j} b_{3/2}^{(1)}\left(\frac{a_j}{a_p}\right), \tag{B17}$$

with $a_< \equiv \min(a_j, a_k)$ and $a_> \equiv \max(a_j, a_k)$.

In the strong-coupling limit, with $|\hat{\boldsymbol{l}}_j - \hat{\boldsymbol{l}}_k| \ll 1$, the total angular momentum of the inner binary, $\boldsymbol{L} = L\hat{\boldsymbol{l}} = \sum_j \boldsymbol{L}_j$, evolves according to Eq. (13), with the precession rate given by

$$\Omega_L \simeq \frac{1}{L}\sum_j L_j \Omega_{jp}. \tag{B18}$$

In the corotating frame of $\boldsymbol{L}$, the evolution of $\Delta\boldsymbol{l}_j = \hat{\boldsymbol{l}}_j - \hat{\boldsymbol{l}}$ is governed by the equation

$$\left(\frac{\mathrm{d}\Delta\boldsymbol{l}_j}{\mathrm{d}t}\right)_{\rm rot} \simeq -\sum_{k\neq j}\omega_{jk}\hat{\boldsymbol{l}}\times(\Delta\boldsymbol{l}_j - \Delta\boldsymbol{l}_k) + (\Omega_{jp} - \Omega_L)(\hat{\boldsymbol{l}}\cdot\hat{\boldsymbol{l}}_p)(\hat{\boldsymbol{l}}\times\hat{\boldsymbol{l}}_p). \tag{B19}$$

We can recast Eq. (B19) into a more convenient form. Set up a Cartesian coordinate system, with the z-axis along $\hat{\boldsymbol{l}}$ and the y-axis along $\hat{\boldsymbol{l}}\times\hat{\boldsymbol{l}}_p$. Let $\Delta\boldsymbol{l}_j = (\Delta l_j)_x\hat{\boldsymbol{x}} + (\Delta l_j)_y\hat{\boldsymbol{y}}$, and define the complex variable

$$I_j \equiv (\Delta l_j)_x + i(\Delta l_j)_y. \tag{B20}$$

Then Eq. (B19) reduces to (suppressing the subscript "rot")

$$\frac{\mathrm{d}I_j}{\mathrm{d}t} = -i\sum_k A_{jk}I_k + iB_j, \tag{B21}$$

where

$$A_{jk} = \Big(\sum_n \omega_{jn}\Big)\delta_{jk} - \omega_{jk}, \tag{B22}$$

$$B_j = (\Omega_{jp} - \Omega_L)\sin\theta_p\cos\theta_p. \tag{B23}$$

We can write Eq. (B21) in a more compact form:

$$\frac{\mathrm{d}\boldsymbol{Y}}{\mathrm{d}t} = -i\boldsymbol{A}\cdot\boldsymbol{Y} + i\boldsymbol{B}, \tag{B24}$$

where the $N\times N$ matrix has the element A_{jk}, and

$$\boldsymbol{Y} = \begin{pmatrix} I_1 \\ I_2 \\ \vdots \\ I_N \end{pmatrix}, \quad \boldsymbol{B} = \begin{pmatrix} B_1 \\ B_2 \\ \vdots \\ B_N \end{pmatrix}. \tag{B25}$$

In the absence of the external perturber, $B_j = 0$, Eq. (B21) or (B24) describes the free inclination oscillations of the N-planet system (Murray & Dermott 1999). The eigenmodes $\boldsymbol{Y}_\alpha$ ($\alpha = 1, 2, \cdots, N$) of these free oscillations satisfy the equation

$$\lambda_\alpha\boldsymbol{Y}_\alpha = \boldsymbol{A}\cdot\boldsymbol{Y}_\alpha, \tag{B26}$$

where λ_α is the eigenvalue, with $\boldsymbol{Y}_\alpha \propto \exp(-i\lambda_\alpha t)$.

The general solution of Eq. (B24) takes the form

$$\boldsymbol{Y}(t) = \boldsymbol{A}^{-1}\cdot\boldsymbol{B} + \sum_\alpha c_\alpha\boldsymbol{Y}_\alpha\exp(-i\lambda_\alpha t), \tag{B27}$$

where the constants c_α's are determined by the initial condition. Assuming $\boldsymbol{Y}(t=0) = 0$, we have

$$c_\alpha = -\boldsymbol{Y}_\alpha^\dagger\cdot\boldsymbol{A}^{-1}\cdot\boldsymbol{B}, \tag{B28}$$

where the eigenvector $\boldsymbol{Y}_\alpha$ has been normalized by

$$\boldsymbol{Y}_\alpha^\dagger\cdot\boldsymbol{Y}_\beta = \delta_{\alpha\beta}. \tag{B29}$$

The mutual inclination in the N-planet system is measured by

$$\frac{1}{N}\sum_j\left|\hat{\boldsymbol{l}}_j\times\hat{\boldsymbol{l}}\right|^2 = \frac{1}{N}\sum_j|I_j(t)|^2 = \frac{1}{N}\Big|\boldsymbol{Y}(t)\Big|^2. \tag{B30}$$

Using Eq. (B27), we then have

$$\left\langle\frac{1}{N}\sum_j\left|\hat{\boldsymbol{l}}_j\times\hat{\boldsymbol{l}}\right|^2\right\rangle = \frac{1}{N}\Big[\Big|\boldsymbol{A}^{-1}\cdot\boldsymbol{B}\Big|^2 + \sum_\alpha|c_\alpha|^2\Big]. \tag{B31}$$

REFERENCES

Albrecht, S., et al. 2013, ApJ, 771, 11
Ballard, S., Johnson, J.A. 2016, ApJ, 816, 66
Baranec, C., et al. 2016, AJ, 152, 18
Becker, J.C., Adams, F.C. 2016, MNRAS, 455, 2980
Becker, J.C., et al. 2015, ApJ, 812, L18
Boue, G., Fabrycky, D.C. 2014, ApJ, 789, 110
Bryan, M., et al. 2016, ApJ, 821, 89
Campante, T.L., et al. 2015, ApJ, 799, 170
Chatterjee, S., Ford, E.B., Matsumura, S., Rasio, F.A. 2008, ApJ, 686, 580,
Coughlin, J.L., et al. 2016, ApJS, 224, 12
Cumming, A., et al. 2008, PASP, 120, 531
Dai, F., et al. 2015, ApJ, 813, L9
Dawson, R.I., Fabrycky, D.C. 2010, ApJ, 722, 937
Dupuy, T.J., et al. 2016, ApJ, 817, 80
Fabrycky, D.C., et al. 2014, ApJ, 790, 146
Fang, J., Margot, J.-L. 2012, ApJ, 761, 92
Fang, J., Margot, J.-L. 2013, ApJ, 767, 115
Feng, Y.K., et al. 2015, ApJ, 800, 22
Figueira, P., et al. 2012, A&A, 541, A139
Foucart, F., Lai, D. 2011, MNRAS, 412, 2799
Foucart, F., Lai, D. 2014, MNRAS, 445, 173
Gettel, S., et al. 2016, ApJ, 816, 95
Gilliland, R.L. et al. 2013, ApJ, 766, 40
Hale, A. 1994, AJ, 107, 306
Hansen, B.M.S, & Murray, N. 2013, ApJ, 775, 53
Huber, D., et al. 2013, Science, 342, 331
Johansen, A., Davies, M.B., Church, R.P., Holmelin, V. 2012, ApJ, 758, 39
Juric, M., Tremaine, S. 2008, ApJ, 686, 603
Kraus, A.L., et al. 2016, AJ, 152, 8
Lai, D. 2014, MNRAS, 440, 3532

Lissauer, J.J., et al. 2011, ApJS, 197, 8
Liu, B., Munoz, D.J., Lai, D. 2015, MNRAS, 447, 747
Marcy, G.W., et al. 2014, ApJ, 210, 20
Marmier, M., et al. 2013, A&A, 551, 90
McArthur, B.E., et al. 2004, ApJ, 614, L81
Moriarty, J., Ballard, S. 2015, arXiv:1512.03445
Morton, T.D., et al. 2016, ApJ, 822, 86
Morton, T.D., Winn, J.N. 2014, ApJ, 796, 47
Moutou, C., et al. 2015, A&A, 576, 48
Mullally, F., et al. 2015, ApJS, 217, 31
Murray, C.D., Dermott, S.F. 1999, Solar System Dynamics (Cambridge Univ. Press)
Neveu-VanMalle, M., et al. 2016, A&A, 586, 92
Ngo, H., et al. 2016, ApJ, in press (arXiv:1606.07102)
Oter, O.J., et al. 2016, arXiv:1608.03627
Pu, B., Wu, Y. 2015, ApJ, 807, 44
Rowan, D., et al. 2016, ApJ, 817, 104
Schmitt, J.R., et al. 2014, AJ, 148, 28
Tremaine S. 1991, Icarus, 89, 85
Tremaine S., Dong, S. 2012, AJ, 143, 94
Tremaine S., Touma J., Namouni F., 2009, AJ, 137, 3706
Uehara, S., et al. 2016, ApJ, 822, 2
Veras, D., Armitage, P.J. 2004, Icarus, 172, 349
Volk, K., Gladman, B. 2015, ApJ, 806, L26
Wang, J., Fischer, D.A., Horch, E.P., Xie, J.-W. 2015a, ApJ, 806, 248
Wang, J., Fischer, D.A., Xie, J.-W., Ciardi, D.R. 2015b, ApJ, 813, 130
Weissbein, A., Steinberg, E., Sari, R. 2012, arXiv:1203.6072
Wittenmyer, R.A., et al. 2014, 791, 114
Wittenmyer, R.A., et al. 2016, ApJ, 819, 28
Xie, J.-W., Wu, Y., Lithwick, Y. 2014, ApJ, 789, 165
Xie, J.-W., et al. 2016, arXiv:1609.08633